Analysis of Helicopter Rotor Blade Stall Flutter

Peter Crimi*
Avco Systems Division, Wilmington, Mass.

A study of rotor blade aeroelastic stability is carried out, using an analytic model of a two-dimensional airfoil undergoing dynamic stall and an elastomechanical representation including flapping, flapwise bending, and torsional degrees of freedom. Results for a hovering rotor demonstrate that the models are capable of reproducing both classical and stall flutter. The minimum rotor speed for the occurrence of stall flutter in hover is found to be determined from coupling between torsion and flapping. Instabilities analogous to both classical and stall flutter are found to occur in forward flight. However, the large stall-related torsional oscillations which commonly limit aircraft forward speed appear to be the response to rapid changes in aerodynamic moment which accompany stall and unstall, rather than the result of an aeroelastic instability.

Nomenclature

b = blade semichord
$\bar{C}_L$ = mean lift coefficient, ratio of time average of l to $\rho\Omega^2R^2b$
C_l = lift coefficient, $C_l = l/(\rho U^2 b)$
$C_{m\,c/4}$ = moment coefficient referred to quarterchord, $C_{m\,c/4} = m_{c/4}/(2\rho U^2 b^2)$
c = blade chord
h_i = translational coordinates of 2-D system (i = 1, 2), semichords
I_o = moment of inertia of 2-D system about pitch axis
k_i = translational spring stiffnesses of 2-D system (i = 1, 2)
k_θ = torsional spring stiffness of 2-D system
l = lift per unit span at aerodynamic reference radius
l_{si} = offsets of springs from pitch axis of 2-D system (i = 1, 2)
$m_{c/4}$ = aerodynamic moment per unit span at aerodynamic reference radius
m_i = masses of 2-D system, i = 1, 2
R = rotor radius
r_o = inner radius of blade lifting surface
r_R = aerodynamic reference radius
U = instantaneous free-stream speed at aerodynamic reference section
U_o = reference speed, $U_o = \Omega r_R$
x_m = distance aft of elastic axis of blade section mass center
$\bar{x}$ = distance aft of pitch axis of mass center of m_1
Z_β = generalized coordinate of 2-D system, equivalent to tip displacement due to flapping, semichords
Z_ϕ = generalized coordinate of 2-D system, equivalent to tip displacement due to bending, semichords
α = angle of attack
θ_o = collective pitch angle
θ_1 = angular displacement of 2-D system, equivalent to tip displacement due to torsion, rad
$\tilde{\theta}$ = angle of zero restraint of 2-D system torsion spring
μ = advance ratio, ratio of forward speed to ΩR
ρ = freestream density
ψ = blade azimuth angle measured from downwind direction
Ω = rotor rotational speed
Ω^* = dimensionless rotor speed, $\Omega^* = \Omega R/(\omega_{\theta_o} b)$
ω_f = flutter frequency
ω_{θ_o} = frequency of first uncoupled, nonrotating torsion mode
$\omega_{\phi o}$ = frequency of first uncoupled, nonrotating flapwise bending mode

Presented as Paper 73-403 at the AIAA/ASME/SAE 14th Structures, Structural Dynamics, and Materials Conference, Williamsburg, Va., March 20–22, 1973; submitted April 24, 1973; revision received February 21, 1974. This study was jointly sponsored by NASA and the U.S. Army under Contract NAS1-11378.

Index categories: Aeroelasticity and Hydroelasticity; VTOL Vibration.

*Senior Consulting Scientist. Member AIAA.

Introduction

AEROELASTIC stability of a helicopter rotor blade is a multifaceted problem because of the extreme variations of the aerodynamic environment within the flight envelope of the aircraft. In hovering flight, a blade can undergo classical binary flutter[1] or stall flutter.[2] In forward flight, the linear instability experienced by systems with periodically varying parameters can occur.[3] While these types of instability are not normally encountered with blades of current design, because of the relatively low disk loading and weak coupling of translational and rotational degrees of freedom, they are certainly not precluded from new designs, particularly those intended to extend present performance capabilities. Of immediate concern, however, in both design and operation, is the occurrence of large-amplitude torsional oscillations and excessive control-linkage loads associated with blade stall on the retreating side of the rotor disk at high forward speed or gross weight, effectively limiting aircraft performance. This problem has prompted a number of recent studies of dynamic stall and the effects of stall on blade dynamics.[4–8]

While stall has been identified as a causal element of the problem, the nonlinearity of the stall process, coupled with the unsteady aerodynamic environment, has precluded an analysis to the depth required to gain a thorough understanding of the mechanisms involved. In particular, it has not been clear whether the blade undergoes a true aeroelastic instability, a simple forced response, or some hybrid phenomenon which takes on the character of one or the other extreme, depending on flight conditions and blade vibrational characteristics.

Stall flutter for axial flight is amenable to analysis by empirical methods similar to those developed for analyzing stall flutter in cascades.[9] The flutter mechanism for that case has been identified as deriving from the extraction of energy from the free stream by the periodic variation of the aerodynamic moment. Analogous methods applied to the forward-flight problem[10,11] have been inconclusive, however, the primary difficulty possibly being in applying empirical methods without a clear definition of the underlying mechanism of the problem.

A method was recently developed for analyzing dynamic stall of an airfoil undergoing arbitrary pitching and plunging motions which provides an ideal tool for analyzing the stall problem in forward flight. The method, which is described in detail in Ref. 7, employs models for each of the basic flow elements contributing to the unsteady stall of a two-dimensional airfoil, without recourse to empiricism.

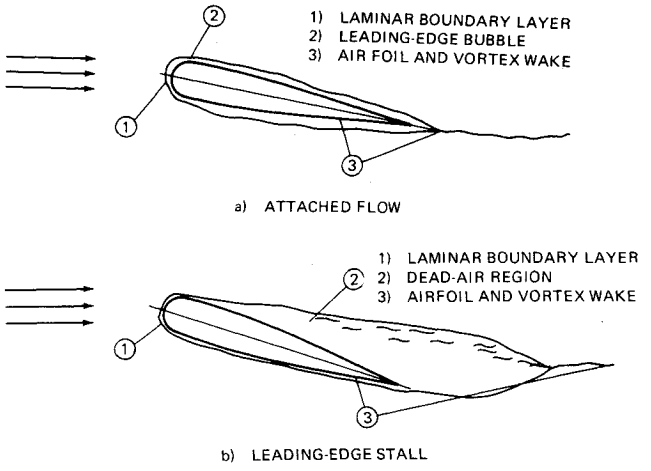

Fig. 1 Flow elements.

Calculations of the loading during transient and sinusoidal pitching motions are in good qualitative agreement with measured loads. Dynamic overshoot, or lift in excess of the maximum static value, as well as unstable moment variation, are in clear evidence in the computed results.

This study was directed to analyzing the aeroelastic stability of a helicopter rotor, particularly as it relates to stall, using the method of Ref. 7 to compute aerodynamic loading. The representation of the elastomechanical system includes flapping and flapwise-bending degrees of freedom as well as torsion.

Problem Formulation

Aerodynamic Loading

In the flutter analysis, only leading-edge stall was considered, so the following relates specifically only to that type, even though the basic method can treat trailing-edge stall as well. When the airfoil is not stalled, the flow elements represented are (see Fig. 1a): 1) the laminar boundary layer from the stagnation point to separation near the leading-edge, 2) the small leading-edge separation bubble; and, 3) a potential flow, including a vortex wake generated by the variation with time of the circulation about the airfoil. When the airfoil is stalled, as indicated in Fig. 1b, the flow elements are: 1) the laminar boundary layer, 2) a dead-air region extending from the separation point to the pressure recovery point; and, 3) a potential flow external to the airfoil and dead-air region, again including a vortex wake. The analytic representations of these elements are described briefly below. Details are given in Ref. 7.

Potential Flow

Given the airfoil section characteristics and motions, together with the distribution of pressure in the dead-air region if the airfoil is stalled, the flow and pressure over the airfoil must be determined to compute the integrated load and analyze the boundary layer. The problem was formulated by imposing linearized boundary conditions of flow tangency and pressure, using a perturbation velocity potential derived from source and vortex distributions. The resulting coupled set of singular integral equations is solved by casting the singularity distributions in series form and solving for the unknown coefficients by imposing boundary conditions at prescribed points.

Boundary Layer

Because the relative importance of the individual elements of the boundary-layer flow as they affect dynamic stall could not be established in advance, the representation in Ref. 7 was made as general as possible. The method of finite differences for unsteady flows with variable step size in both streamwise and normal directions was employed, with the error in each finite-difference approximation the order of the square of the step size. It was determined from preliminary calculations performed for this study that, at least for leading-edge stall, results are virtually unaffected by assuming quasi-steady flow in the boundary layer. That assumption was therefore employed for all flutter computations, to take advantage of the resulting substantial savings in computer storage requirements and computing time.

Dead Air Region

The function of the model of the dead-air region is to define the streamwise distribution of pressure in that region, given the locations of the separation and recovery points and the pressure at the recovery point. The dead-air region is assumed to consist of a laminar constant-pressure free shear layer from separation to transition, a turbulent constant-pressure mixing region, and a turbulent pressure-recovery region. The laminar shear layer is analyzed by the method of Ref. 12, assuming quasi-steady flow. There is no direct justification for the assumption of quasi-steady flow, but the results of the boundary-layer analyses do indicate that it is probably a reasonable one. The turbulent mixing and pressure-recovery regions are analyzed using the steady-flow momentum integral and first moment equations. Profile parameters in these regions are assumed to be universal functions of a dimensionless streamwise coordinate, with those functions derived from an exact viscous-inviscid interaction calculation. Matching of approximate solutions for the mixing and pressure-recovery regions at their interface completes the analysis.

Leading-Edge Bubble

The leading-edge bubble on an unstalled airfoil is analyzed using the same basic relations employed for the dead-air region. Given the boundary-layer parameters at separation, the length of the bubble and the amount of pressure rise possible, for that length, in the pressure recovery region, are computed. That pressure rise is compared with the rise in pressure in the potential flow over the length of the bubble. If the latter is greater than the former, the bubble is assumed to have burst, and the stall process is initiated.

Loading Calculation Procedure

Calculations proceed by forward integration in time, using the blade motions derived by integrating the equations of motion of the elastomechanical system. If, at a given instant, the airfoil is not stalled, the potential flow is computed, and the boundary-layer and leading-edge bubble are analyzed to check for bubble bursting. If the airfoil is stalled, the pressure distribution in the dead-air region is computed, the potential flow evaluated, and the boundary layer is analyzed to locate the separation point. The last two steps are repeated iteratively until assumed and computed separation points agree. Rate of growth of the dead-air region is determined from an estimate of the rate of fluid entrainment derived from the potential-flow solution. Unstall is determined by first postulating its occurrence and analyzing the leading-edge bubble which

would then form to ascertain whether that event did in fact occur. During unstall, the dead-air region is washed off the airfoil at the freestream speed.

Elastomechanical Representation

The equations of motion for a rotor blade with flapping, flapwise bending, and torsional degrees of freedom can be written in the form[3]

$$\sum_{j=1}^{3}(M_{ij}\ddot{q}_j - \Omega^2 T_{ij} q_j) + K_i q_i = F_i \quad i = 1,2,3$$

where q_1 is tip displacement due to flapping, q_2 is tip displacement due to first-mode bending, and q_3 is angular tip displacement due to first-mode torsion. The uncoupled natural frequencies of those degrees of freedom are then given, respectively, by

$$\omega_\beta^2 = -\Omega^2 T_{11}/M_{11} \quad (K_1 = 0),$$

$$\omega_\phi^2 = \omega_{\phi_o}^2 - \Omega^2 T_{22}/M_{22} \quad (\omega_{\phi_o}^2 = K_2/M_{22}),$$

$$\omega_\theta^2 = \omega_{\theta_o}^2 - \Omega^2 T_{33}/M_{33} \quad (\omega_{\theta_o}^2 = K_3/M_{33})$$

The generalized mass and centrifugal-force coefficients are integrals over the blade span involving the blade inertial properties and vibrational mode shapes (see, for example, Ref. 3).

The complexity of the aerodynamic representation described in the previous section precludes evaluation of the generalized forces by the usual strip approximation. It was felt essential, however, to retain both of the translational degrees of freedom in the investigation of the forward-flight problem, so a simple two-dimensional model of the dynamics could not be used. Therefore, a two-dimensional airfoil suspended in such a way as to have three degrees of freedom was analyzed. Inertial and stiffness parameters were assigned to make the coupled natural frequencies of the two-dimensional system match those of the rotor blade.

The system analyzed is shown schematically in Fig. 2. The system is seen to differ considerably from the usual two-dimensional or representative-section model, which has a single linear spring attached at the same point as the torsion spring (see, for example, Ref. 13). The linear spring with stiffness k_1 is attached a distance l_{s1} from the axis of the torsion spring. Also, a mass m_2 has been connected to the primary inertial elements through a spring k_2. The motion of mass m_2, while not contributing directly to the aerodynamic loading, provides a second translational degree of freedom. The spring attachment offsets l_{s_1}, and l_{s_2} are needed to reproduce the static coupling due to centrifugal effects in the rotor blade equations of motion.

The matching of the two-dimensional system with the blade dynamics proceeds as follows. Three generalized coordinates are first defined to correspond to those of the blade. Clearly, angular displacement θ_1 should correspond to blade torsional displacement at the blade tip. The counterparts of flapping and bending, Z_β and Z_ϕ, respectively, are defined by

$$Z_\beta = A_1 h_1 + B h_2, \quad Z_\phi = A_2 h_1 - B h_2$$

where

$$A_1 = \frac{\omega_\beta^2 - \omega_2^2}{\omega_\phi^2 - \omega_\beta^2}, \quad A_2 = \frac{\omega_2^2 - \omega_\phi^2}{\omega_\phi^2 - \omega_\beta^2}$$

$$B = \frac{(\omega_2^2 - \omega_\phi^2)(\omega_2^2 - \omega_\beta^2)}{(\omega_\phi^2 - \omega_\beta^2)\omega_2^2} \tag{1}$$

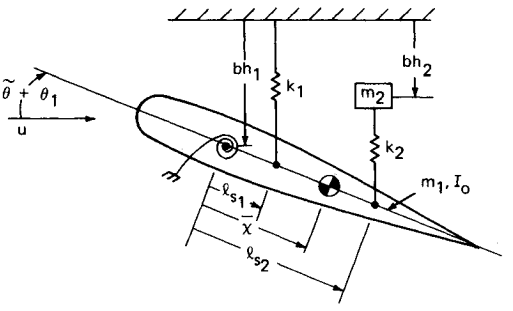

Fig. 2 Two-dimensional elastomechanical system.

and $\omega_i^2 = k_i/m_i$, $i = 1, 2$. With the above definitions, $Z_\beta + Z_\phi = -h_1$, to give the correct translational correspondence. It can further be shown that the uncoupled natural frequencies of the two-dimensional system match those of the blade, provided

$$(k_\theta + k_1 l_{s_1}^2 + k_2 l_{s_2}^2)/I_o = \omega_\theta^2$$

while

$$\omega_1^2 \text{ and } \omega_2^2 \text{ satisfy}$$

$$\omega_1^2 \omega_2^2 = \omega_\phi^2 \omega_\beta^2 .$$

$$\omega_1^2 + (1 + m_2/m_1)\omega_2^2 = \omega_\phi^2 + \omega_\beta^2 \tag{2}$$

By comparing the generalized masses of the two systems, it follows that

$$m_1 b^2/I_o = -A_1 M_{11} b^2/(M_{33} R^2)$$

$$A_2/A_1 = M_{11}/(M_{22} R^2) \equiv \lambda_m$$

The last relation, together with Eqs. (1) and (2), fixes m_2/m_1:

$$m_2/m_1 = \frac{(1 + \lambda_m)(\omega_\phi^4 + \lambda_m \omega_\beta^4)}{(\lambda_m \omega_\beta^2 + \omega_\phi^2)^2} - 1$$

Equating the corresponding coefficients of the characteristic equations of the two systems provides three additional relations, which can be solved for the coupling parameters $\bar{x}$, l_{s_1}, and I_{s_2}.

To complete the matching, quasi-steady approximations to the damping terms of the flapping equations are equated with the result that

$$m_1 R/(-A_1) = 4 \frac{r_R}{R} \frac{M_{11}}{R^2[1 - (r_o/R)^4]}$$

$$U/U_o = 1 + \frac{4}{3}\left[\frac{1 - (r_o/R)^2}{1 - (r_o/R)^4}\right] \mu \sin\psi$$

where $\Omega r_R = U_o$. The aerodynamic reference radius r_R was selected to be $0.75R$.

Analysis Procedure

The equations of motion of the two-dimensional system were solved by integrating analytically, using linear extrapolations to approximate the variations of lift and aerodynamic moment over the interval of integration. More specifically, given the values of lift 1 at times t_1 and $t_1 - \Delta t$, it was assumed that $l(t) = l(t_1) + [l(t_1) - 1(t_1 - \Delta t)](t - t_1)/\Delta t$ over the interval from t_1 to $t_1 + \Delta t$, and similarly for the aerodynamic moment. With the lift and aerodynamic moment prescribed analytically in this form,

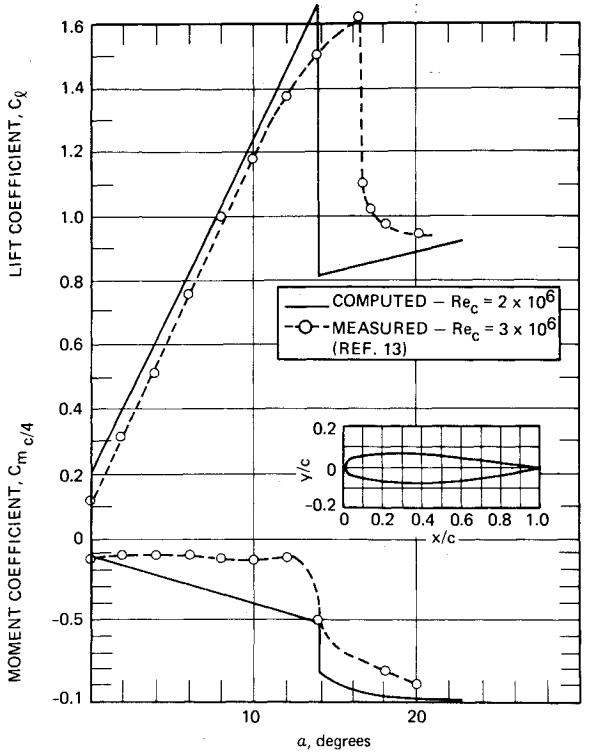

Fig. 3 Airfoil section characteristics for NACA 23012.

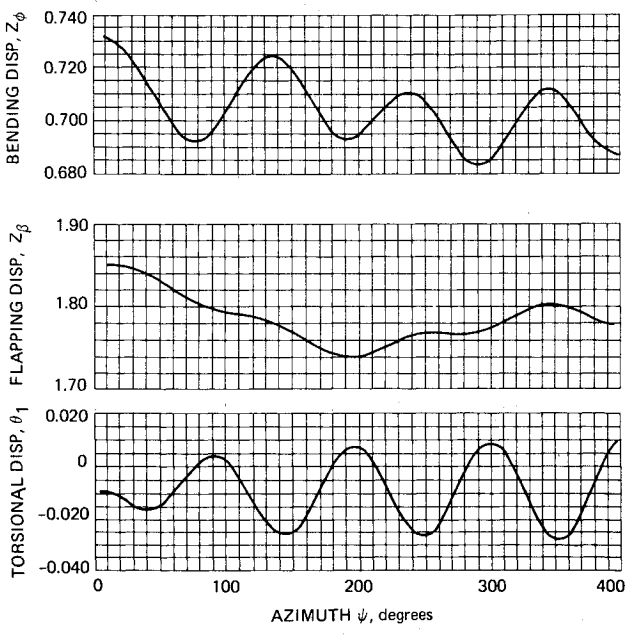

Fig. 4 Displacement time histories at classical flutter onset: $\Omega^* = 5.3$, $\theta_o = 11°$, $\mu = 0$.

the equations of motion are readily solved to provide the plunging rate h_1, pitch angle θ_p and pitch rate θ_p at time $t_1 + \Delta t$. Those quantities were in turn employed to compute corrected values for the lift and moment at that instant, using the previously described aerodynamic representation. The scheme was found to give satisfactory results, provided the time interval of integration Δt is no longer than about one fifth of the period of the coupled mode having the highest natural frequency.

The angle of zero restraint in torsion was varied periodically to approximate the effects of cyclic pitch variation in forward flight, according to the formula

$$\tilde{\theta} = \theta_o[1 - 2(R/r_R)\mu \sin \psi]$$

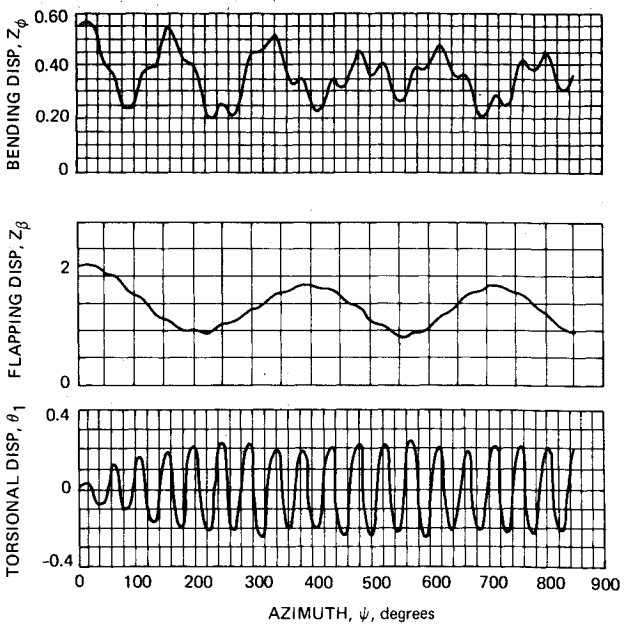

Fig. 5 Displacement time histories for stall flutter: $\Omega^* = 3.1$, $\theta_o = 15°$, $\mu = 0$.

Results of Computations

Configuration Analyzed

Vibrational and aerodynamic characteristics of the blade analyzed were selected to correspond to those of the model rotor blade described in Ref. 2. That blade is untwisted, of constant chord, with $b/R = 0.0435$, $r_o/R = 0.174$, $\omega_{\theta_o}/\omega_{\phi_o} = 3.69$ and $x_m/b = 0.216$.

The test blade had a NACA 23012 section. The variation of static lift and moment coefficients with angle of attack for this section were computed from a series of transient pitch calculations, and are shown in Fig. 3, together with the measured section characteristics from Ref. 14. The aerodynamic model is seen to give nearly the correct maximum lift but at a slightly lower angle of attack, and as indicated from the variation of $C_{m\ c/4}$, the computed center of pressure is somewhat further aft than that of the actual airfoil section below the stall angle.

Stability in Hover

Initial calculations were performed for hovering flight, to allow a direct comparison with the test results of Ref. 2 and to verify that the analytic models are capable of reproducing both classical and stall flutter. First, rotor speed was varied parametrically, with the collective pitch at a value well below the stall incidence. A classical bending-torsion instability was encountered at $\Omega^* = \Omega R/(\omega_{\theta_o} b) = 5.3$ with $\omega_f/\omega_\theta = 0.803$. The variation of bending, flapping, and torsional displacements with azimuth angle at flutter onset are shown in Fig. 4. By way of comparison, tests[2] yielded classical flutter at about $\Omega^* = 7.1$ with $\omega_f/\omega_{\theta_o} = 0.72$. These differences between analysis and test results can be attributed in large part to the use of a two-dimensional aerodynamic model, which cannot precisely reproduce the aerodynamic coupling between the rotational and translational degrees of freedom.

Susceptibility of the system to stall flutter was investigated next. It was found that a torsional limit cycle, at approximately the highest coupled natural frequency of the system, could be triggered for Ω^* as low as 3.4. Computed blade motions for stall flutter at $\Omega^* = 3.5$ are shown in Fig. 5.

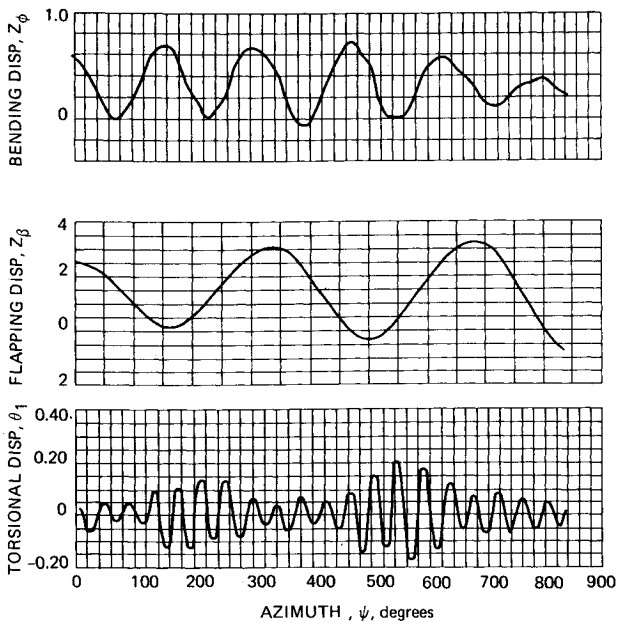

Fig. 6 Blade Response Below Stall Flutter Boundary: $\Omega^* = 3.1$, $\theta_o = 15°$, $\mu = 0$.

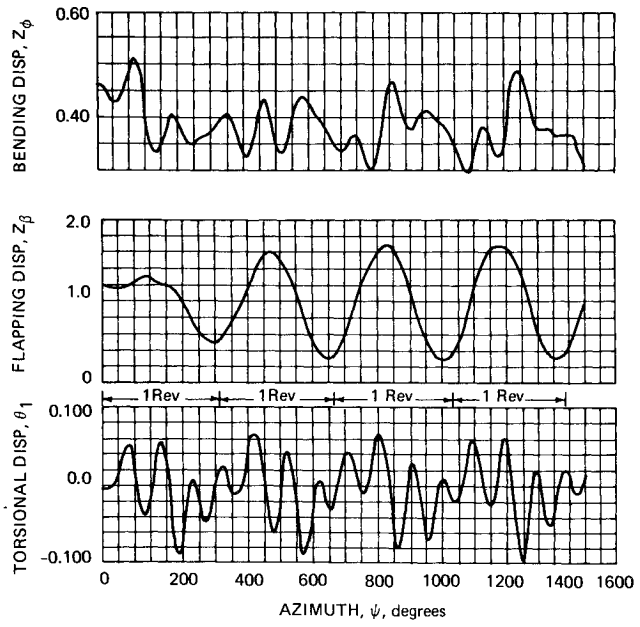

Fig. 7 Displacement time histories at linear instability onset: $\Omega^* = 5.2$, $\theta_o = 6°$, $\mu = 0$.

For Ω^* below 3.4 a well-defined limit cycle could not be set up, regardless of the initial conditions or the collective pitch angle. Severe oscillations involving repeated stall and unstall could be made to occur by imposing a large initial bending deflection. However, the flapping response modulated the torsional response, and caused continuous stall and/or unstall of the blade over a significant portion of a revolution, due to the large plunging rate generated by the flapping motion. An example of this occurrence is shown in Fig. 6. Note the gradual damping of the bending oscillations and the build-up of the flapping motion in Fig. 6, neither of which occur during stall flutter (Fig. 5). Thus, while stall flutter involves only the rotational degree of freedom, the results obtained indicate that the minimim speed for its occurrence is determined by coupling with a translational degree of freedom.

Stability in Forward Flight

The blade was analyzed next for an advance ratio μ of 0.1. Computations were carried out in the same sequence as for hovering. First, the rotational speed at which classical flutter occurs was determined. Then, stall-related instabilities were investigated.

A linear bending-torsion instability of the Floquet type[15] was encountered at $\Omega^* = 5.2$. Blade motions as a function of azimuth angle at flutter onset are shown in Fig. 7. The torsional and bending displacements are seen to display the aperiodic character typical of this type of instability. The flapping motion is the steady-state response to the cyclic pitch variation.

An instability analogous to stall flutter in hover was found to occur for Ω^* as low as about 4.4, with collective pitch angle greater than 12 deg. Blade motions for $\Omega^* = 4.8$ are shown in Fig. 8. The torsional displacement time history, while not strictly periodic, is nonetheless brought about by successive stall and unstall. The azimuth positions at which those events occur are marked by *(S)* and *(U)*, respectively, on the ψ-scale.

The blade motions for the type of instability shown in Fig. 8 are not of the same character as those of particular concern in the limiting of helicopter performance, in that the excessive torsional displacements shown in Fig. 8 persist over a complete revolution of the blade. The control

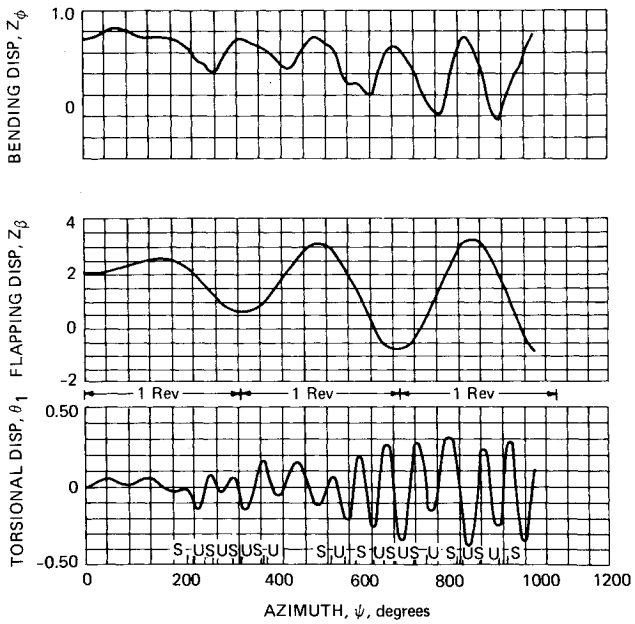

Fig. 8 Displacement time histories for stall flutter: $\Omega^* = 4.8$, $\theta_o = 13°$, $\mu = 0.1$.

load time history, taken from flight test,[6] shown in Fig. 9 illustrates the type of stall-related blade motions usually encountered at a thrust level or forward speed near the upper limit of an aircraft. Large oscillations in the control loads, presumably deriving from blade torsional oscillations, are seen from Fig. 9 to persist only between about $\psi = 270°$ and $\psi = 400°$, rather than throughout a complete revolution of the blade.

A torsional displacement time history closely resembling the variation of control loads in Fig. 9 was obtained for Ω^* less than 4.4, for collective pitch angles between 12 and 13°. Results for a typical case are shown in Fig. 10. The occurrences of stall and unstall are indicated on the abscissas. The large oscillations in torsion are clearly related to stall, but their persistence is not the result of successive stalling and unstalling, as would be the case for true stall flutter. The blade appears to be responding to

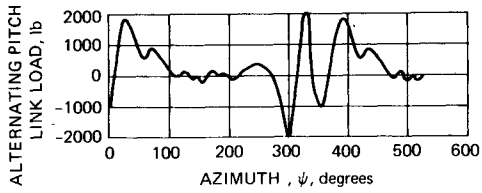

Fig. 9 Variation of pitch link load in flight test of CH-47 at 123 knots (from Ref. 6).

the sudden changes in aerodynamic moment at stall onset and unstall, as can be seen by comparing the variation of moment coefficient shown in Fig. 10 with that of torsional displacement, and noting the azimuth positions at which stall and unstall occur. There is some cyclic stall-unstall within the stall zone evident in the results on the second and third revolutions. However, the major contributors to the oscillations appear to be the initial and final pulses associated with stall and unstall upon entering and leaving that zone. There are, in general, two cycles of torsional oscillation of excessive amplitude after the blade unstalls the last time on a given revolution. The severity of the response is apparently due, in part, to the suddenness of load changes at stall and partly to the relative lack of aerodynamic damping in pitch, particularly when the blade is not stalled.

It could be argued that the blade torsional oscillations of Fig. 10 are still a manifestation of stall flutter, even though successive stall and unstall is not taking place, since the aerodynamic moment can undergo unstable variations when the blade remains stalled throughout a cycle.[4] It may, in fact, be the case that the large deflections do result partly from that effect, so choosing to term them as simply a response may be somewhat misleading.

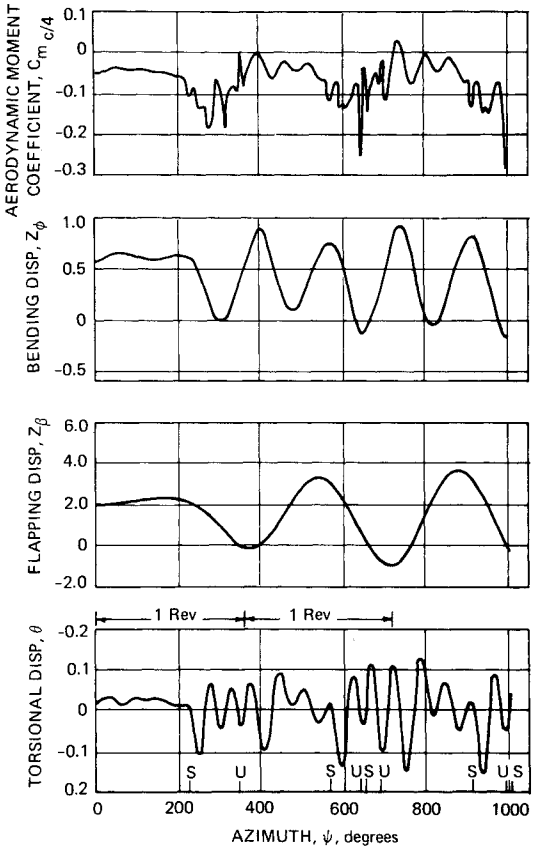

Fig. 10 Displacement and moment time histories for excessive torsional response: $\Omega^* = 3.89$, $\theta_o = 12°$, $\mu = 0.1$.

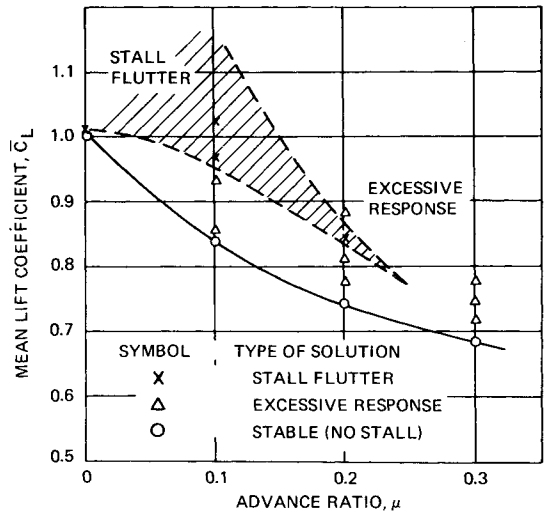

Fig. 11 Stall stability boundaries for $\Omega^* = 3.89$.

On the other hand, the solutions are distinctly different from what is definitely stall flutter obtained both in hover (Fig. 5) and in forward flight (Fig. 8), so that label would seem to be even less appropriate. Further, the persistence of the oscillations after exit from the stall zone is clearly symptomatic of a response, so for lack of a more precise term, solutions of the type shown in Fig. 10 are identified in what follows as excessive response.

Stall Flutter and Response Boundaries

The effect of forward speed on stall-related instabilities was investigated by systematically varying the collective pitch angle and advance ratio, with Ω^* equal to 3.89. In order to relate the results to rotor performance, a mean lift coefficient $\bar{C}_L$ is defined, according to

$$\bar{C}_L = \bar{l}/\rho\Omega^2 R^2 b$$

where $\bar{l}$ is the time-averaged lift per unit span at the aerodynamic reference radius. This coefficient is, to a good approximation, directly proportional to the thrust coefficient.[16]

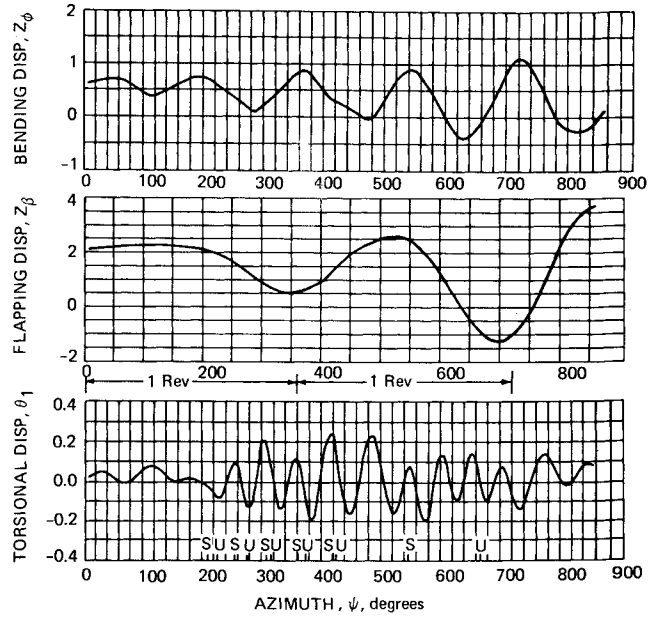

Fig. 12 Displacement time histories at high advance ratio: $\Omega^* = 3.89$, $\bar{C}_L = 0.78$, $\mu = 0.3$.

The results obtained are summarized in Fig. 11 as a plot of $\overline{C}_L$ vs μ. As thrust is increased at a given μ, the rotor is seen to first encounter a region of excessive response, of the type discussed previously, and then, for μ of 0.2 or less, a region where stall flutter occurs. Increasing advance ratio has the effect of suppressing the tendency for stall flutter. At $\mu = 0.2$, stall flutter occurs at $\overline{C}_L = 0.85$, but a further increase in $\overline{C}_L$ results in excessive response again. At $\mu = 0.3$ a limit-cycle type of oscillation could not be triggered at all. As a result, stall flutter is confined to a region somewhat as indicated by the shaded area in Fig. 11.

The supression of stall flutter at high advance ratio is apparently caused by an effect similar to the one encountered at low rotor speed in hover, whereby the flapping motion prevented a limit cycle from occurring. This can be seen from the blade motions obtained for $\mu = 0.3$ and $\overline{C}_L = 0.78$, plotted in Fig. 12. On the first revolution, as the blade enters the stall zone on the retreating side, it appears that a limit cycle is being set up, with repeated stall and unstall occurring. However, at about $\psi = 420°$, the flapping motion has built up in response to the large cyclic pitch changes, producing a negative plunging rate sufficient to keep the blade unstalled over the remainder of its passage on the advancing side. Then, when the blade again enters the stall zone, the large positive flap-induced plunging rate precludes unstall until exit from the stall zone at about $\psi = 670°$. As a result, the blade subsequently undergoes excessive torsional response, rather than stall flutter.

References

[1]DuWaldt, F., Gates, C., and Piziali, R., "Investigation of Helicopter Rotor Blade Flutter and Flapwise Bending Response in Hovering," WADC Tech. Rept. 59-403, Aug. 1959; Wright-Air Development Center, Wright-Patterson Air Force Base, Ohio.

[2]Brooks, G. W. and Baker, J. E., "An Experimental Investigation of the Effects of Various Parameters Including Tip Mach Number on the Flutter of Some Model Helicopter Rotor Blades," TN 4005, Sept. 1958, NACA.

[3]Daughaday, H., DuWaldt, F., and Gates, C., "Investigation of Helicopter Blade Flutter and Load Amplification Problems," *Journal of the American Helicopter Society,* Vol. 2, No. 3, July 1957; also IAS Preprint No. 705, Jan. 1957.

[4]Liiva, J., et al., "Two-Dimensional Tests of Airfoils Oscillating Near Stall," USAAVLAB Tech. Rept. 68-13A, April 1968, U.S. Army Aviation Material Lab., Ft. Eustis, Va.

[5]Ericsson, L. and Reding, J., "Dynamic Stall of Helicopter Blades," *Journal of the American Helicopter Society,* Vol. 17, No. 1, Jan. 1972, pp. 11–19.

[6]Tarzanin, F., "Prediction of Control Loads Due to Blade Stall," *Journal of the American Helicopter Society,* Vol. 17, No. 2, April 1972, pp. 33–46.

[7]Crimi, P. and Reeves, B. L., "A Method for Analyzing Dynamic Stall of Helicopter Rotor Blades," CR-2009, May 1972, NASA.

[8]Johnson, W. and Ham, N. D., "On the Mechanism of Dynamic Stall," *Journal of the American Helicopter Society,* Vol. 17, No. 4, Oct. 1972, pp. 36–45.

[9]Sisto, F., "Stall Flutter in Cascades," *Journal of the Aeronautical Sciences,* Vol. 20, No. 9, Sept. 1953, pp. 598–604.

[10]Carta, F. O. and Niebanck, C. F., "Prediction of Rotor Instability at High Forward Speeds, Vol. III: Stall Flutter," USAAVLABS Tech. Rept. 68-18C, Feb. 1969, U.S. Army Aviation Material Lab., Ft. Eustis, Va.

[11]Ham, N. D. and Young, M. I. "Torsional Oscillation of Helicopter Blades Due to Stall," *Journal of Aircraft,* Vol. 3, No. 3, May–June 1966, pp. 218–224.

[12]Reeves, B. L. and Lees, L., "Theory of Laminar near Wake of Blunt Bodies in Hypersonic Flow," *AIAA Journal,* Vol. 3, No. 11, Nov. 1965, pp. 2061–2074.

[13]Fung, Y. C., *The Theory of Aeroelasticity,* Wiley, New York, 1955, p. 227.

[14]Abbott, I. H. and von Doenhoff, A. E., *Theory of Wing Sections,* Dover, New York, 1959.

[15]Crimi, P., "Stability of Dynamic Systems with Periodically Varying Parameters," *AIAA Journal,* Vol. 8, No. 10, Oct. 1970, pp. 1760–1764.

[16]Gessow, A. and Meyers, G., *The Aerodynamics of the Helicopter,* Ungar, New York, 1967.